ELSEVIER

Journal of Fluids and Structures 20 (2005) 853–869

JOURNAL OF FLUIDS AND STRUCTURES

www.elsevier.com/locate/jfs

Numerical simulation of self-oscillations of human vocal folds with Hertz model of impact forces

J. Horáček[a,*], P. Šidlof[a], J.G. Švec[b]

[a]*Institute of Thermomechanics, Academy of Sciences of the Czech Republic, Dolejškova 5, 182 00 Prague 8, The Czech Republic*
[b]*Medical Healthcom Ltd., Centre for Communication Disorders, Řešovská 10/491, 181 00 Prague 8, The Czech Republic*

Received 10 September 2004; accepted 6 May 2005
Available online 14 July 2005

Abstract

A mathematical model was developed previously (by Horáček and Švec in 2002a) for studying the influence of the geometrical, viscoelastic and vibrational characteristics of the human vocal folds on their self-sustained oscillations in phonatory air-flow. That model is advanced here by: (i) extending the equations for unsteady aerodynamic forces from small to realistic vibrational amplitudes of the vocal folds; (ii) implementing the Hertz model of impact forces for vocal-fold collisions; (iii) adjusting the elastic support of the vocal-fold-shaped vibrating element for more flexible tuning of the natural frequencies of vibrations; and (iv) moving from frequency domain calculations towards on-line simulations in the time domain. Using a parabolic vocal-fold shape and vocal-fold natural frequencies close to 100 Hz, the model exhibits vibrations for flow velocities, flow volumes and subglottal pressures above 0.5 m/s, 0.1 l/s, and 0.15 kPa, respectively. During collisions, the model reveals impact stress values up to 3 kPa. As these values are close to those measured in humans, the model is found suitable for studying phenomena and estimating values, which are difficult to observe and measure in the living vocal folds.

Keywords: Flow induced vibrations; Human voice biomechanics; Post-critical behaviour

1. Introduction

Vibrations of vocal folds are of extraordinary importance for production of human voice. As the vocal folds are difficult to study in vivo, the mathematical and numerical models could be very helpful for understanding the mechanism of voice production. First lumped-parameters dynamic models of the vocal-fold self-oscillations were developed already at the beginning of seventies of the last century (Ishizaka and Flanagan, 1972) and their different variations remain to be widely used (Liljencrants, 1991; Pelorson et al., 1994; Herzel and Knudsen, 1995; Story and Titze, 1995; Lous et al., 1998; De Vries et al., 1999; Ikeda et al., 2001). New versions of the self-oscillating vocal-fold models have been described during the last 2 years (LaMar et al., 2003; Sciamarella and d'Alessandro, 2004; Adachi and Yu, 2005; Drioli, 2005).

A short overview of numerous existing models can be found, e.g., in the dissertation of Kob (2002). A frequent problem of the developed mathematical models is the relationship of their input parameters to the real material

*Corresponding author. Tel.: +420 2 66053125; fax: +420 2 8584695.
E-mail address: jaromirh@it.cas.cz (J. Horáček).

0889-9746/$ - see front matter © 2005 Elsevier Ltd. All rights reserved.
doi:10.1016/j.jfluidstructs.2005.05.003

properties of the vocal folds and to the aerodynamic properties of the phonatory airstream. The aerodynamic forces have usually been approximated by quasi-steady forces given by the Bernoulli law. The latest finite-element models developed for vibration of the vocal folds in viscous fluid flow described by the Navier–Stokes equations (Thomson et al., 2003; Alipour et al., 2000) are still in a preliminary phase and their reliability and usability for an on-line numerical simulation of the vocal-fold self-oscillations with impacts is limited. A sufficiently accurate description of unsteady viscous fluid flow characteristics measured on oscillating rigid replicas of vocal folds during their collisions appears problematic (Deverge et al., 2003). Similar problems of flow-induced vibrations for flows in collapsible tubes were studied, e.g., by Cancelli and Pedley (1985), where the dominant mechanism for self-sustained vibrations relied on flow separation and a pressure recovery downstream of the narrowest section of the tube.

The authors have developed a linear aeroelastic model in order to study the influence of different geometrical and elastic properties of the vocal folds on phonation thresholds (Horáček and Švec, 2002a, b). An inviscid incompressible 1-D fluid flow theory was used in the model for expressing the unsteady aerodynamic forces and the parameters of the model, i.e., the mass, stiffness and damping matrices were approximately related to the geometry, size and material density of real vocal folds as well as to the known or prescribed fundamental natural frequencies and damping. In the current paper, the model is advanced by: (i) extending the equations for unsteady aerodynamic forces from small perturbations to realistic vibrational amplitudes; (ii) implementing the Hertz model of impact forces for vocal fold collisions; (iii) improving the tuning possibilities of the natural frequencies of the vocal folds by replacing the continuous elastic foundation by a two-spring elastic support; and (iv) moving from frequency domain calculations towards on-line simulations in the time domain. First the mathematical model is formulated and the solution procedures are presented, then the results of the on-line simulations are demonstrated, and finally the model behaviour is related to the real vocal folds by comparing its output data to values measured in living subjects.

2. Mathematical model

The model of the glottis with the vocal folds is shown in Fig. 1 as a channel with planar symmetry conveying air. The length of the channel, L, is measured parallel to both the plane of symmetry and the direction of air-flow.

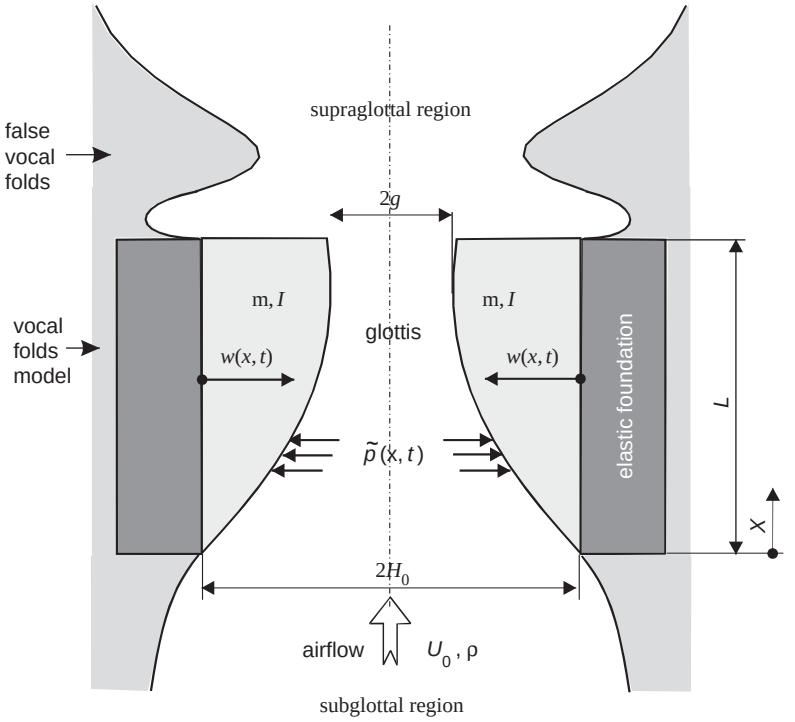

Fig. 1. Schematic of the glottal space.

The channel walls are created by two vocal-fold-shaped rigid bodies of mass m and moment of inertia I, which are vibrating symmetrically in the opposite phase with identical amplitudes on an elastic foundation. The rigid bodies oscillate in the fluid of density ρ flowing in the channel with the mean flow velocity U_0 at the inlet ($x = 0$), where the cross-section of the channel equals $2H_0$. The minimum cross-section of the channel for a steady state at zero air-flow, the so-called glottal width, is denoted by $2g$ (Fig. 1). The vibrating element has a smooth convergent glottal inlet and a short, not highly divergent, outlet, which is terminated with a sharp edge at which the flow separation occurs. Symmetric oscillations of the vocal folds are assumed, allowing modelling only a half of the glottal region (Fig. 2(a)).

2.1. Equations of motion for the vocal-fold-shaped vibrating element

The vocal fold can be approximated by a two-degree-of-freedom rigid body element with a defined shape $a(x)$, where x is the axial coordinate. The element is supported by two discrete springs with stiffnesses c_1 and c_2 (Fig. 2) and its vibration is described by its rotation and translation. An equivalent three-mass system can be used to formulate the equations of motion of the element, based on the three conditions of identical total mass, static moment and moment of inertia of the rigid body. The vibrating rigid body with mass m, moment of inertia I, and the centre of gravity T at the

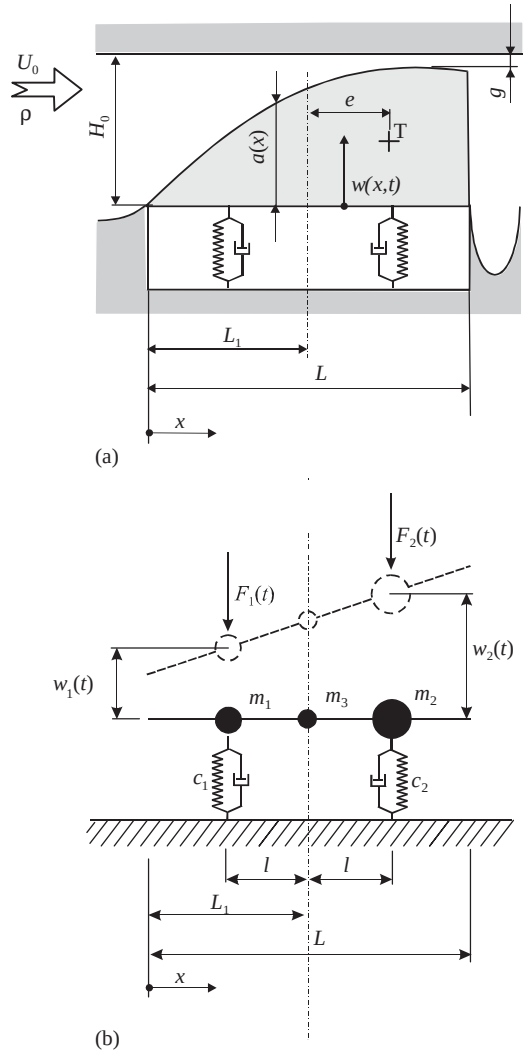

Fig. 2. Two-degree-of-freedom model.

location e (the eccentricity—see Fig. 2(a)) is replaced by the masses

$$m_{1,2} = \frac{1}{2l^2}(I + me^2 \mp mel), \quad m_3 = m\left[1 - \left(\frac{e}{l}\right)^2\right] - \frac{I}{l^2} \tag{1}$$

joined together by a rigid massless rod of the total length L. The distance between the masses m_1 and m_2 is denoted as $2l$ and the distance L_1 from the upstream end of the rod defines their position (see Fig. 2(b)). The displacements of the masses m_1 and m_2 are denoted as $w_1(t)$ and $w_2(t)$, where t is time. The length L should approximately correspond to the anatomical data; the lengths l and L_1 can, however, be varied for the purpose of tuning of the model.

The displacement of the rigid massless rod can be written as

$$w(x,t) = (x - L_1)V_1(t) + V_2(t), \tag{2}$$

where the rotation and translation of the rigid body element was introduced as

$$V_1(t) = \frac{w_2(t) - w_1(t)}{2l}, \quad V_2(t) = \frac{w_2(t) + w_1(t)}{2}. \tag{3}$$

When the glottis is open, the force and moment equilibrium equations can be used to express the equivalent excitation aerodynamic forces $F_1(t)$ and $F_2(t)$ acting on the vocal folds (Fig. 2(b))

$$F_1(t) = \frac{h}{2}\int_0^L \left(1 - \frac{x}{l} + \frac{L_1}{l}\right)\tilde{p}(x,t)\,\mathrm{d}x, \quad F_2(t) = \frac{h}{2}\int_0^L \left(1 + \frac{x}{l} - \frac{L_1}{l}\right)\tilde{p}(x,t)\,\mathrm{d}x, \tag{4}$$

where h is the width of the channel (identical with the width of the rigid body) and $\tilde{p}(x,t)$ is the air pressure along the vibrating body surface. The width of the channel is measured perpendicular to the direction of air-flow and parallel to the plane of symmetry.

After expressing the potential and kinetic energies of the system in a similar way as in the previous article (Horáček and Švec, 2002a) and their substitution in the Lagrange equations, the equations of motion are obtained in the form

$$\mathbf{M}\ddot{\mathbf{V}} + \mathbf{B}\dot{\mathbf{V}} + \mathbf{K}\mathbf{V} + \mathbf{F} = 0, \tag{5}$$

where the following displacement and excitation force vectors were introduced

$$\mathbf{V} = \begin{bmatrix} V_1(t) \\ V_2(t) \end{bmatrix}, \quad \mathbf{F} = \begin{bmatrix} F_1(t) \\ F_2(t) \end{bmatrix} \tag{6}$$

and where $\mathbf{M}, \mathbf{B}, \mathbf{K}$ are the structural mass, damping and stiffness matrices

$$\mathbf{M} = \begin{bmatrix} -lm_1 & m_1 + \dfrac{m_3}{2} \\ +lm_2 & m_2 + \dfrac{m_3}{2} \end{bmatrix}, \quad \mathbf{B} = \varepsilon_1\mathbf{M} + \varepsilon_2\mathbf{K}, \quad \mathbf{K} = \begin{bmatrix} -c_1 l & c_1 \\ +c_2 l & c_2 \end{bmatrix}. \tag{7}$$

The damping matrix $\mathbf{B}$ represents a proportional model of structural damping; $\varepsilon_1, \varepsilon_2$ are constants adjusted hereafter according to the desired damping ratios for the two natural modes of vibration of the system. The structure of the matrices $\mathbf{M}$ and $\mathbf{K}$ reveals that a mass coupling caused by the mass m_3 is generally in the system even if $\mathbf{F} = 0$.

2.2. Aerodynamic unsteady forces for open glottis

The unsteady continuity and 1-D Euler equations for incompressible fluid can be used to express the aerodynamic forces acting on the vibrating element (Norton, 1989; Horáček and Švec, 2002a). The equation for unsteady pressure in the glottis was derived in a linear form by Horáček and Švec (2002a, p. 937, Eq. (16)) supposing only small flow velocity perturbations ($\tilde{u}\partial\tilde{u}/\partial x \to 0$). Here, we generalize the equation by incorporating also the nonlinear term $\tilde{u}\partial\tilde{u}/\partial x$. Using the velocity potential $\Phi(x,t)$ for the unsteady component of the flow velocity $\tilde{u}(x,t) = \partial\Phi(x,t)/\partial x$, the unsteady component of the pressure can be formulated in a nonlinear form as

$$\tilde{p}(x,t) = -\rho\left[\frac{\partial\Phi}{\partial t} + \bar{U}(x)\frac{\partial\Phi}{\partial x} + \frac{1}{2}\left(\frac{\partial\Phi}{\partial x}\right)^2\right], \tag{8}$$

where the mean (steady) flow velocity in the glottis for $x \in \langle 0, L\rangle$ can be expressed from the continuity equation as

$$\bar{U}(x) = U_0/[1 - a(x)/H_0]. \tag{9}$$

Using the boundary conditions for the flow at the inlet ($x = 0$) and outlet ($x = L$)

$$\tilde{u} = \partial\Phi/\partial x = 0|_{x=0} \quad \text{and} \quad \tilde{p} = 0|_{x=L}, \tag{10}$$

considering the displacement $w(x,t) \ll H_0$ and using the same procedure as in the previous paper (Horáček and Švec, 2002a, pp. 937–938, Eqs. (9)–(10)) the unsteady component of the pressure can be written as

$$\begin{aligned}\tilde{p}(x,t) = & -\rho\{K_1(x)[V_1(t)]^2 + K_2(x)V_2(t) + K_3(x)[V_2(t)]^2 + K_4(x)[\dot{V}_1(t)]^2 + K_5(x)\dot{V}_2(t) + K_6(x)V_2(t)\dot{V}_2(t) \\ & + K_7(x)[\dot{V}_2(t)]^2 + K_8(x)\dot{V}_1(t) + K_9(x)\dot{V}_1(t)V_1(t) + K_{10}(x)\dot{V}_1(t)V_2(t) + K_{11}(x)\dot{V}_1(t)\dot{V}_2(t) + K_{12}(x)V_1(t) \\ & + K_{13}(x)V_1(t)V_2(t) + K_{14}(x)V_1(t)\dot{V}_2(t) + K_{15}(x)\ddot{V}_1(t) + K_{16}(x)\ddot{V}_2(t)\},\end{aligned} \tag{11}$$

where the coefficients $K_i(x)(i = 1, 2, \ldots, 16)$ are complicated functions, which are specified in Appendix A. The general forms of Eq. (11) for pressure as well as the coefficients $K_i(x)$ were calculated by using the symbolic manipulation capabilities of the software *Mathematica*.

Then, the aerodynamic forces $F_1(t)$ and $F_2(t)$ can be expressed as nonlinear functions of the displacements $V_1(t)$ and $V_2(t)$ by calculating the integrals (4). Using the *Mathematica* for numerical integration of the coefficients $K_i(x)$ the resulting aerodynamic forces exciting the vocal folds are obtained for open glottis:

$$\begin{aligned}F_1(t) = & -\rho\{K_1^{\text{int }1}[V_1(t)]^2 + K_2^{\text{int }1}V_2(t) + K_3^{\text{int }1}[V_2(t)]^2 + K_4^{\text{int }1}[\dot{V}_1(t)]^2 + K_5^{\text{int }1}\dot{V}_2(t) + K_6^{\text{int }1}V_2(t)\dot{V}_2(t) \\ & + K_7^{\text{int }1}[\dot{V}_2(t)]^2 + K_8^{\text{int }1}\dot{V}_1(t) + K_9^{\text{int }1}\dot{V}_1(t)V_1(t) + K_{10}^{\text{int }1}\dot{V}_1(t)V_2(t) + K_{11}^{\text{int }1}\dot{V}_1(t)\dot{V}_2(t) + K_{12}^{\text{int }1}V_1(t) \\ & + K_{13}^{\text{int }1}V_1(t)V_2(t) + K_{14}^{\text{int }1}V_1(t)\dot{V}_2(t) + K_{15}^{\text{int }1}\ddot{V}_1(t) + K_{16}^{\text{int }1}\ddot{V}_2(t)\},\end{aligned} \tag{12}$$

$$\begin{aligned}F_2(t) = & -\rho\{K_1^{\text{int }2}[V_1(t)]^2 + K_2^{\text{int }2}V_2(t) + K_3^{\text{int }2}[V_2(t)]^2 + K_4^{\text{int }2}[\dot{V}_1(t)]^2 + K_5^{\text{int }2}\dot{V}_2(t) \\ & + K_6^{\text{int }2}V_2(t)\dot{V}_2(t) + K_7^{\text{int }2}[\dot{V}_2(t)]^2 + K_8^{\text{int }2}\dot{V}_1(t) + K_9^{\text{int }2}\dot{V}_1(t)V_1(t) + K_{10}^{\text{int }2}\dot{V}_1(t)V_2(t) \\ & + K_{11}^{\text{int }2}\dot{V}_1(t)\dot{V}_2(t) + K_{12}^{\text{int }2}V_1(t) + K_{13}^{\text{int }2}V_1(t)V_2(t) + K_{14}^{\text{int }2}V_1(t)\dot{V}_2(t) + K_{15}^{\text{int }2}\ddot{V}_1(t) + K_{16}^{\text{int }2}\ddot{V}_2(t)\},\end{aligned} \tag{13}$$

where the following notation was introduced:

$$K_i^{\text{int }1} = h\int_0^L K_i(x)\frac{l + L_1 - x}{2l}\,\mathrm{d}x \text{ and } K_i^{\text{int }2} = h\int_0^L K_i(x)\frac{l - L_1 + x}{2l}\,\mathrm{d}x, \quad i = 1, \ldots, 16. \tag{14}$$

2.3. Model of the vocal-fold collisions

The Hertz model of impact (Brepta and Prokopec, 1972; Stronge, 2000; Půst and Peterka, 2003) is implemented here to account for vocal-fold collisions. The impact force F_H is considered as

$$F_H = k_H\delta^{3/2}(1 + b_H\dot{\delta}), \quad k_H \cong \frac{4}{3}\frac{E}{1 - \mu_H^2}\sqrt{r}, \tag{15}$$

where δ is the penetration of the vocal-fold element through the contact plane (see Fig. 3), E is Young's modulus, μ_H is the Poisson ratio, b_H is a damping factor and r is the radius of curvature of the impacting body surfaces approximated by the shape $a(x)$ of the vocal-fold model in the contact point according to the equation

$$\frac{1}{r} = \frac{|\mathrm{d}^2a/\mathrm{d}x^2|}{\left[1 + (\mathrm{d}a/\mathrm{d}x)^2\right]^{3/2}}. \tag{16}$$

The geometry of the vocal fold is approximated by a general parabolic function:

$$a(x) = a_1x + (a_2/2)x^2. \tag{17}$$

The moving surface of the vibrating vocal-fold element (see Fig. 3) is described by the function

$$y(x,t) = a(x) + w(x,t) = a(x) + (x - L_1)V_1(t) + V_2(t), \quad x \in \langle 0, L\rangle. \tag{18}$$

From here the coordinates of the contact point can be determined as

$$\begin{aligned}x_{\max}(t) &= \min\{L, \max[0, -[V_1(t) + a_1]/a_2]\}, \\ y_{\max}(t) &= y[x_{\max}(t)] = a[x_{\max}(t)] + [x_{\max}(t) - L_1]V_1(t) + V_2(t).\end{aligned} \tag{19}$$

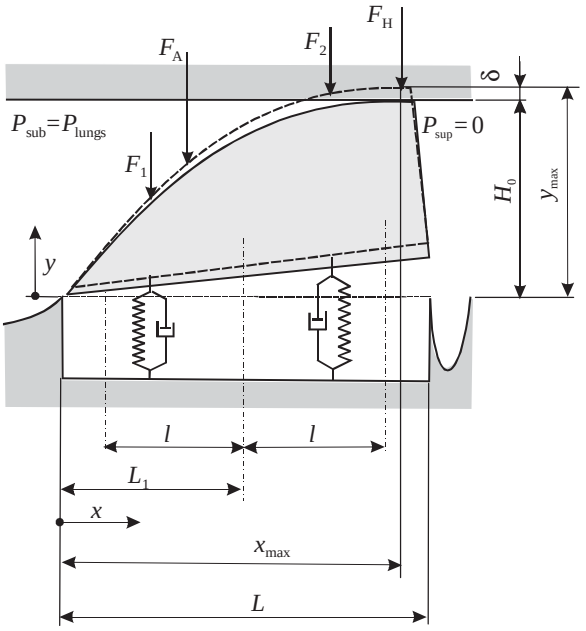

Fig. 3. Schema of the model for the closed glottis when the vocal-fold-shaped element is loaded by a resulting aerodynamic force F_A and the Hertz contact force F_H.

Using these equations, the Hertz impact force (15) can be rewritten (see Fig. 3) in the form

$$F_H(t) = k_H[y_{\max}(t) - H_0]^{3/2}, \tag{20}$$

where the damping factor b_H in the contact is neglected.

During the impact, when the glottis is closed, the aerodynamic forces (12) and (13) are switched off. There are three types of forces acting on the vocal-fold-shaped element during this time (Fig. 3): (i) the Hertz force, Eq. (20); (ii) the subglottal pressure P_{sub}, which is acting on the subglottal part of the element surface (this pressure equals the lungs pressure P_{lungs} and is kept steady as the lungs are considered a big air reservoir ($P_{\text{lungs}} = P_{\text{sub}} = const.$); and (iii) the supraglottal pressure, which is acting on the supraglottal part of the element surface. That pressure is set here to zero ($P_{\text{sup}} = 0$).

After integration of the pressure $P_{\text{sub}} = P_{\text{lungs}}$ in the interval $x \in \langle 0, x_{\max}(t)\rangle$, the aerodynamic force can be expressed as $F_A(t) = P_{\text{sub}} x_{\max}(t) h$. Finally, the resulting forces in the equations of motion (5) during vocal-fold contact (see Figs. 2 and 3) can be approximated as

$$\begin{aligned} F_1(t) &= F_H(t)\frac{L_1 + l - x_{\max}(t)}{2l} + P_{\text{sub}} h x_{\max}(t)\frac{L_1 + l - x_{\max}(t)/2}{2l}, \\ F_2(t) &= F_H(t)\frac{x_{\max}(t) - L_1 + l}{2l} + P_{\text{sub}} h x_{\max}(t)\frac{x_{\max}(t)/2 - L_1 + l}{2l}. \end{aligned} \tag{21}$$

3. Numerical solution

3.1. Solution of the linearized problem—computation of stability boundaries

For calculating the stability boundaries, only small vibration amplitudes without collisions and small velocity perturbations ($\tilde{u}\partial\tilde{u}/\partial x \to 0$) can be considered. In this case, the perturbation pressure (8) is given by the simplified equation

$$\tilde{p} = -\rho\left(\frac{\partial \Phi}{\partial t} + \bar{U}(x)\frac{\partial \Phi}{\partial x}\right). \tag{22}$$

That results in a substantial simplification of Eq. (11) for the pressure

$$\tilde{p}(x,t) = -\rho \left[\begin{array}{l} \ddot{V}_1(t)K_{15}(x) + \ddot{V}_2(t)K_{16}(x) + \dot{V}_1(t)K_8(x) + \dot{V}_2(t)K_5(x) \\ \quad + V_1(t)K_{12}(x) + V_2(t)K_2(x) \end{array} \right]. \tag{23}$$

Subsequently, the linear approximation of the forces $F_{1,2}(t)$ is given by Eqs. (12) and (13), where only the corresponding constants $K_i^{\text{int}\,1}, K_i^{\text{int}\,2}$ $(i = 2, 5, 8, 12, 15, 16)$ are not equal to zero.

Substituting the linearized aerodynamic forces $F_{1,2}(t)$ in the equations of motion (5) and dividing this equation by $ml/2$ yields the following physically well-structured equations of motion of the coupled aeroelastic system in a linear approximation:

$$\bar{\mathbf{M}}\ddot{\bar{\mathbf{V}}} + \bar{\mathbf{B}}\dot{\bar{\mathbf{V}}} + \bar{\mathbf{K}}\bar{\mathbf{V}} = \frac{\rho h L^3}{m H_0}\left[\hat{\mathbf{M}}\ddot{\bar{\mathbf{V}}} + \frac{U_0}{L}\hat{\mathbf{B}}\dot{\bar{\mathbf{V}}} + \frac{U_0^2}{L^2}\hat{\mathbf{K}}\bar{\mathbf{V}}\right], \tag{24}$$

where

$$\bar{\mathbf{M}} = \begin{bmatrix} -\left(\dfrac{I}{ml^2} + \left(\dfrac{e}{l}\right)^2 - \dfrac{e}{l}\right) & \left(1 - \dfrac{e}{l}\right) \\ +\left(\dfrac{I}{ml^2} + \left(\dfrac{e}{l}\right)^2 + \dfrac{e}{l}\right) & \left(1 + \dfrac{e}{l}\right) \end{bmatrix}, \quad \bar{\mathbf{B}} = \bar{\varepsilon}_1\bar{\mathbf{M}} + \bar{\varepsilon}_2\bar{\mathbf{K}}, \quad \bar{\mathbf{K}} = \Omega_0^2 \begin{bmatrix} -1 & 1 \\ \underline{c_2} & \underline{c_2} \\ c_1 & c_1 \end{bmatrix} \tag{25}$$

are the dimensionless mass, damping and stiffness matrices for the rigid body vibrating in vacuo, $\Omega_0^2 = 2c_1/m$. The expression

$$\bar{\mathbf{V}} = \begin{bmatrix} 1 & 0 \\ 0 & 1/l \end{bmatrix}\mathbf{V} \tag{26}$$

gives the vector of dimensionless displacements. The elements in the matrices of the aerodynamic mass $\hat{\mathbf{M}}$, damping $\hat{\mathbf{B}}$ and stiffness $\hat{\mathbf{K}}$, which are complicated functions of the channel geometry, are specified in an analytical form for the special case $L_1 = L/2$ in Appendix B.

The unsteady aerodynamic forces on the right-hand side of Eq. (24) are obviously proportional to the dimensionless added mass of fluid $(\rho h L^3/mH_0)$ and they have a lucid physical meaning. The first term corresponds to the aerodynamic inertia forces, the second term to the aerodynamic damping forces $(\sim U_0)$ related to the Coriolis forces, and the third term to the aerodynamic stiffness forces $(\sim U_0^2)$, which are related to the centrifugal forces. The Coriolis and centrifugal forces are increasing functions of the fluid flow velocity U_0, causing aeroelastic instability and self-oscillations.

The numerical procedure for calculation of the stability boundaries from Eq. (24) was presented in the previous paper by Horáček and Švec (2002a) and will only be outlined here. Assuming $\bar{\mathbf{V}} = \bar{\mathbf{V}}_0\,\mathrm{e}^{st}$ for the dynamic response, the solution is given by the numerical computation of the eigenvalues $s = \mathscr{R}e(s) + \mathrm{i}\mathscr{I}m(s)$ and eigenmodes ${}^{\mathrm{T}}\bar{\mathbf{V}}_0 = (V_{01}, V_{02}/l)$ for the eigenvalue problem. In this way, it is possible to calculate the critical flow velocity $U_{0,\text{cirit}}$ at which the real part of the eigenvalue changes the sign from a negative $[\mathscr{R}e(s) < 0]$ to a positive value $[\mathscr{R}e(s) > 0]$. Here, the system either becomes unstable by divergence (when $\mathscr{I}m(s) = 0$), or it becomes unstable by flutter simulating the start of phonation (when $\mathscr{I}m(s) > 0$). The calculated stability boundaries for some of the relevant input parameters of the model are presented in Figs. 4 and 5 (see also Section 5.1).

3.2. Solution for the nonlinear model—simulation of self-oscillations

In order to simulate the postcritical behaviour and study the self-oscillations of the vocal folds, the nonlinear model was used and the numerical solution was implemented in the *Mathematica* 5 (Wolfram, 2003). The equations of motion (5) were transformed into the system of four ordinary first-order differential equations:

$$\dot{Z}_1 = \psi_1(Z_1, Z_2, V_1, V_2), \quad \dot{Z}_2 = \psi_2(Z_1, Z_2, V_1, V_2), \quad \dot{V}_1 = Z_1, \ \dot{V}_2 = Z_2 \tag{27}$$

and a fourth-order standard Runge–Kutta method with adaptive step size was used for the solution. The functions ψ_1, ψ_2 were determined differently for the contact regime (see Eqs. (21)) and the non-contact regime (see Eqs. (12) and (13)). The integrals (14) were pre-calculated for given input data before starting the on-line simulation.

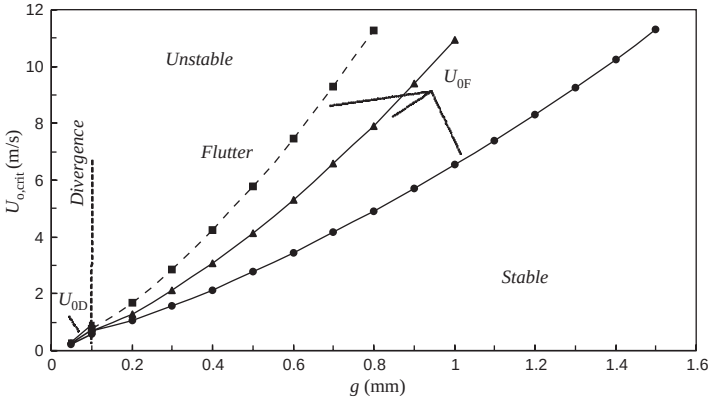

Fig. 4. Stability map for the model with the first natural frequency $f_1 = 100$ Hz and second natural frequency: ---■---, $f_2 = 160$ Hz; —▲—, $f_2 = 130$ Hz; —●—, $f_2 = 105$ Hz.

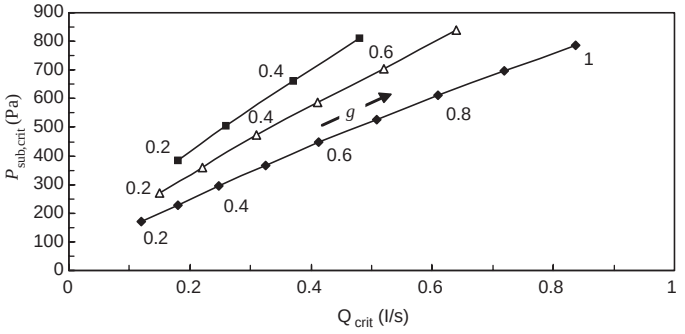

Fig. 5. Calculated critical values (flutter boundaries) for loosing the stability of the vocal fold model. The subglottal pressure $P_{sub.crit}$ and flow rate Q_{crit} for various glottal half-gaps $g = 0.2$–1 mm and for various values of natural frequencies: —◆—, $f_1 = 100$ Hz, $f_2 = 105$ Hz; —△—, $f_1 = 150$ Hz, $f_2 = 155$ Hz; —■—, $f_1 = 200$ Hz, $f_2 = 205$ Hz.

4. Basic input data for numerical analysis

The *input parameters* for the numerical examples and analysis were determined from the published data on the vocal folds [e.g., Titze (1989)]. The density, thickness and length of the vocal folds were taken as follows: $\rho_h = 1020\,\mathrm{kg/m^3}$, $L = 6.8$ mm, $h = 10$ mm. A convex shape $a(x)$ was considered according to Eq. (17), where the dimensionless coefficient $a_1 = 1.858$ and $a_2 = 319.722\,\mathrm{m^{-1}}$ were used. This shape corresponds to the geometry of the vocal fold with an intermediate bulging (Berry et al., 1994). From these data, the parameters needed for construction of the matrix $\tilde{\mathbf{M}}$ were calculated, i.e., the eccentricity $e = 0.77106 \times 10^{-3}$ m, the total mass $m = 2.6731 \times 10^{-4}$ kg and the moment of inertia $I = 1.306 \times 10^{-9}\,\mathrm{kgm^2}$. The air density value of $\rho = 1.2\,\mathrm{kg/m^3}$ was used.

The natural frequencies of the vibrating element and their bandwidths were selected to reflect the experimental data obtained from the true vocal folds (Kaneko et al., 1981, 1983, 1987; Švec et al., 2000). The natural frequencies f_1, f_2 were varied in order to account for different vocal-fold adjustments (examples of some of the values used are shown in Section 5). The 3 dB half-power bandwidths Δf_1 and Δf_2 were fixed to 23 and 29 Hz, respectively. A tuning procedure, based on solving an inverse problem, was used to find the stiffness coefficients c_1, c_2 of the elastic foundation and the damping coefficients $\tilde{\varepsilon}_1, \tilde{\varepsilon}_2$ in the structural matrices $\tilde{\mathbf{B}}$ and $\tilde{\mathbf{K}}$ in Eq. (25). For calculating the coefficients $\tilde{\varepsilon}_1, \tilde{\varepsilon}_2$ for given values Δf_1 and Δf_2, the procedure was the same as described in the previous paper (Horáček and Švec, 2002a). To obtain the complex stiffness coefficients c_1 and c_2 for two prescribed natural frequencies f_1 and f_2, the following two equations were used, which result from the equation of motion (5) for the undamped system ($\mathbf{B} = 0$) vibrating in vacuo ($\mathbf{F} = 0$):

$$[c_1 + (m_1 + m_3/4)(2\pi f_1)^2][c_2 + (m_2 + m_3/4)(2\pi f_1)^2] - (m_3^2/16)(2\pi f_1)^4 = 0 \quad (i = 1, 2). \tag{28}$$

The use of a two-spring elastic support rather than an elastic continuous foundation appeared highly advantageous here, as it enabled tuning of both the natural frequencies (in contrast to only one) and it avoided problems with complex stiffness coefficients experienced in the authors' original model. Symmetric positions of the springs at the distances $L_1 = L/2$ and $l = 0.344L$ (see Fig. 2) were used as these provided optimal tuning possibilities: here both the coefficients c_1, c_2 were real numbers for almost all the ratios $f_2/f_1 > 1.02$. This appears important, as the second natural frequency f_2 of the vocal folds is, in optimal situations, expected to be close to f_1 (Liljencrants, 1991; Berry, 2001). However, the vocal folds could vibrate also when f_2 is higher and further away from f_1 (Ishizaka and Flanagan, 1972; Liljencrants, 1991).

For the impact model, the values $E = 8\,\text{kPa}$ and $\mu_H = 0.4$ (Berry and Titze, 1996; De Vries et al., 1999) were used, which according to Eq. (15) yielded the contact stiffness coefficient $k_H \doteq 730\,\text{N m}^{-2/3}$. The damping in the contact was neglected ($b_H = 0$) in the numerical examples. Finally, the height H_0 of the channel, for a given vocal-fold-shaped element and a glottal half-width g, was expressed as $H_0 = \max_{x\in\langle 0,L\rangle} a(x) + g$ (see Fig. 2(a)).

5. Results of the numerical computations and simulations and their discussion

5.1. Stability map for the linearized model of the vocal-fold vibration

Fig. 4 shows the instability boundaries ($U_{0,\text{crit}}$) of the model as the functions of the glottal half-width g. The boundaries are shown for $f_1 = 100\,\text{Hz}$ and three higher natural frequencies $f_2 = 105\,\text{Hz}$, $f_2 = 130\,\text{Hz}$ and $f_2 = 160\,\text{Hz}$. Two types of instabilities are observed in the model: divergence and flutter. The divergence instability occurs at narrow glottal gaps ($g \lesssim 0.1\,\text{mm}$) above the critical flow velocity U_{0D}. According to the linear approach it results in a suction of the vocal folds together or their abduction without any vibration. The flutter instability takes place when the glottal gap g is wider than approximately 0.1 mm. Here, the vibrations start above the critical flow velocity U_{0F}.

The U_{0F} value is considerably different for the different ratios of the natural frequencies f_2/f_1: when the higher natural frequency f_2 of the system approaches f_1 the instability boundaries for flutter become lower and the initialization of vibrations (and thus the phonation) is easier. As the glottal gap is widened, however, the critical flow velocities U_{0F} generally rise, requiring higher flow values to start the vibrations and making the phonation more difficult.

5.2. Phonation thresholds according to the linear model—comparison of the model to the known in vivo experimental data

The flutter stability boundaries of the model can be related to the phonation threshold values observed in humans. For that, however, it is useful to replace the flow velocity and glottal gap values by the more easily measurable values of the phonation threshold pressure (which corresponds to the critical subglottal pressure $P_{\text{sub,crit}} = P_{\text{lungs}}$) and the phonation threshold air-flow (which corresponds to the critical volume flow rate Q_{crit}). This can be done using the Bernoulli and continuity equations for the steady components of the pressure $\bar{P}(x)$ and the fluid velocity $\bar{U}(x)$

$$P_{\text{lungs}} = \bar{P}(L) + \tfrac{1}{2}\rho\bar{U}^2(L) \quad \text{and} \quad H_0 h U_0 = [H_0 - a(L)]h\bar{U}(L). \tag{29}$$

Assuming $\bar{P}(L) = P_{\text{sup}} = 0$, the following approximate formula can be derived to relate the pressure in lungs to the air-flow velocity:

$$P_{\text{lungs}} = \tfrac{1}{2}\rho U_0^2\{H_0/[H_0 - a(L)]\}^2. \tag{30}$$

The air-flow velocity U_0 (m/s) is simply related to the mean glottal flow volume rate Q (1/s) by the formula:

$$Q = U_0 2H_0 h. \tag{31}$$

Eqs. (30) and (31) relate these quantities to the critical flow velocity for flutter ($U_{0,\text{crit}} = U_{0F}$).

The flutter thresholds are presented in Fig. 5 showing the values of the calculated critical subglottal pressure $P_{\text{sub.crit}}$ (Pa) versus the critical flow rates Q_{crit} (1/s) for various prephonatory glottal half-gaps ($g = 0.2$–$1\,\text{mm}$) and for three different ratios of the natural frequencies ($f_1/f_2 = \frac{100}{105}, \frac{150}{155}$ and $\frac{200}{205}$). The corresponding flutter (fundamental) frequencies F_0 were always found close to the frequencies f_1 and f_2, i.e., $F_0 \simeq 100$, 150 and 200 Hz, respectively. Fig. 5 reveals the critical subglottal pressures and the critical air-flows of the model to be between 0.15 and 0.9 kPa and 0.1 and 0.9 1/s, respectively, which compares well with the range of the values found in humans (Schutte, 1980). The graph shows an increasing threshold pressure value with increasing F_0, which is in agreement with measured data (e.g., Titze, 1992). Also, the increase of the computed subglottal pressure $P_{\text{sub.crit}}$ with the glottal half-width g (see Figs. 4 and 5)

Table 1
The comparison of the expected values P_{th}, Eq. (32) with the computed values $P_{sub,crit}$ from Eq. (24) for phonation thresholds at different fundamental frequencies F_0

F_0 (Hz)	$P_{sub,crit}$ (Pa) (computed—from Eq. (24))	P_{th} (Pa) (formula (32))	
		Males	Females
100	152	182	157
150	270	234	177
200	384	307	206

The glottal half-gap value of $g = 0.2$ mm was used for computation.

corresponds qualitatively to the findings of Chan et al. (1997) in the studies on phonation threshold pressure in a physical model of the vocal-fold mucosa.

A more detailed comparison is offered in Table 1, which relates the model thresholds to the expected phonation threshold values calculated from the formula derived by Titze (1992) and Titze et al. (2003)

$$P_{th} = 0.14 + 0.06(F_0/F_{0N})^2, \tag{32}$$

where F_0 is the fundamental (pitch) frequency and F_{0N} is a nominal (speaking) fundamental frequency ($F_{0N} = 120$ Hz for males and $F_{0N} = 190$ Hz for females). Again, the model values are not far from the expected values, suggesting the model behaviour is in reasonable agreement with reality.

5.3. Simulation of the nonlinear oscillations of the vocal folds in time domain

Whereas the threshold states can be studied with the linear model, studying the postcritical behaviour of the vocal folds including the impacts requires the nonlinear model. A typical starting phase of the on-line simulation is demonstrated in Fig. 6. The input parameters of the simulation example correspond to the unstable (flutter) region in the stability map in Fig. 4 for $f_1 = 100$ Hz and $f_2 = 105$ Hz. The motions $w_1(t)$ and $w_2(t)$ of the masses m_1 and m_2 are shown in the phase plane in Figs. 6(a) and (b), respectively, and in the time domain with a marked impact duration in each vibration period in Figs. 6(c) and (d). Initial conditions: $w_1(0) = w_2(0) = 0.1$ mm and $\dot{w}_1(0) = \dot{w}_2(0) = 0$ for the vocal-fold motion were assumed in this case. The glottal area $S(t)$, i.e., the minimal cross-sectional channel area:

$$S(t) = 2hH(x_{max}(t), t) = 2h[H_0 - y_{max}(t)] \quad \text{for noncontact phase } (y_{max} < H_0),$$

$$S(t) = 0 \quad \text{for contact phase } (y_{max} \geqslant H_0) \tag{33}$$

is shown in the time domain in Fig. 6(e) and the unsteady component of the glottal pressure $p(t) = \bar{p}(x, t)|_{x=L-0.5\,\mathrm{mm}}$ in Fig. 6(f). The spectrum of the glottal pressure, which contains many harmonics, is shown in Fig. 7. The motion of the vocal-fold model during one period of oscillations is animated in Fig. 8.

Fig. 9 shows the dependency of the fundamental vibration frequency $F_0 = 1/T$ (flutter frequency) on the air-flow velocity for three sets of the natural frequencies f_1 and f_2 and for three glottal half gaps g. The resulting F_0 is close to the f_1 and f_2 and slightly increases when increasing the air-flow velocity. Regular self-oscillations with stable F_0 were observed in a wide range of physiologically real input parameters (U_0, g) when the prescribed natural frequencies f_1 and f_2 were close. When the second natural frequency f_2 was increased (e.g. $f_2 = 150$ Hz) while keeping the f_1 at 100 Hz, however, the model revealed rather unstable behaviour with significant hysteresis and sudden jumps between prevailing subharmonic, regular and chaotic oscillations and impactless regimes.

Fig. 10 shows typical behaviour of the aeroelastic model for the natural frequencies $f_1 = 100$ Hz, $f_2 = 105$ Hz and the glottal half-gap $g = 0.3$ mm. The behaviour corresponds to an experiment, in which the flow rate Q was incrementally increased and decreased, and the open quotient OQ (defined as the open time of the glottis divided by the oscillatory period T) was observed. When increasing the flow rate, the self-oscillations occurred above the critical value $Q_{crit} \cong 0.18$ l/s. At the critical value, the vibration pattern was without collisions and $OQ \cong 1$. Above this flow rate ($Q > 0.18$ l/s) the regular self-oscillations with impacts occurred ($OQ < 1$). Further up, above the value of $Q \cong 0.43$ l/s, the vibration regime changed from regular to quasiperiodic (subharmonic), which subsequently changed to chaotic (irregular) once the value of $Q \cong 0.46$ l/s was crossed. For this value the corresponding subglottal pressure $P_{lungs} = 1.3$ kPa, i.e., the so-called phonation instability pressure (Jiang et al., 2003; Jiang and Titze, 1993), was obtained

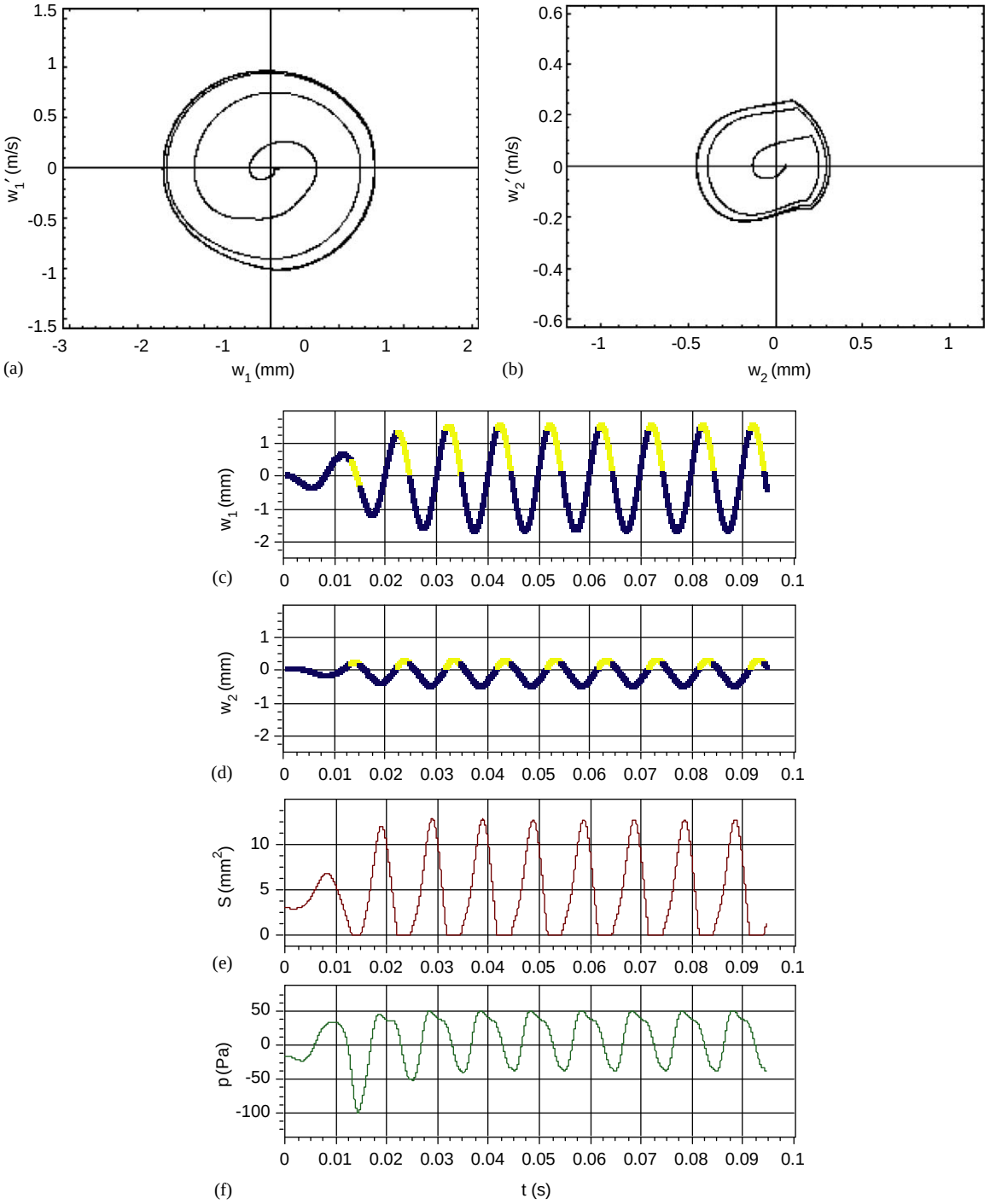

Fig. 6. Example of numerical simulation of the self-oscillations: (a) and (b) phase-plane diagrams for displacement $w_1(t)$ and $w_2(t)$, respectively; (c) and (d) displacements $w_1(t)$ and $w_2(t)$, respectively, with marked impact duration within each period of vibration; (e) glottal area $S(t)$; and (f) glottal pressure $p(t) = \tilde{p}(x,t)|_{x=L-0.5\,\mathrm{mm}}$. The input parameters are the same as in Fig. 4, and the air-flow velocity is $U_0 = 1.6\,\mathrm{m/s}$, glottal half-gap $g = 0.2\,\mathrm{mm}$, prescribed natural frequencies $f_1 = 100\,\mathrm{Hz}$, $f_2 = 105\,\mathrm{Hz}$, time step of numerical integration $\tau = 0.02\,\mathrm{ms}$, mean flow rate $Q = 0.18\,\mathrm{l/s}$ and pressure in lungs $P_{\mathrm{lungs}} = 380\,\mathrm{Pa}$.

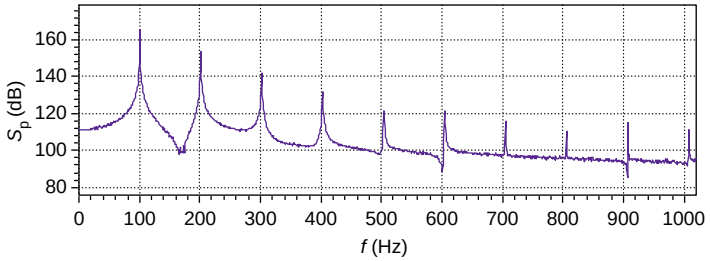

Fig. 7. Spectrum of glottal pressure $\tilde{p}(t) = \tilde{p}(x,t)|_{x=L-0.5\,\mathrm{mm}}$; all parameters as in Fig. 6.

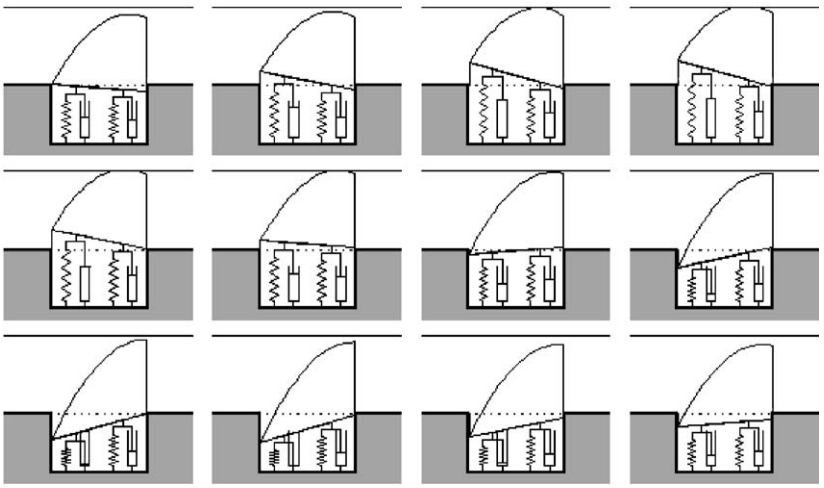

Fig. 8. Phases (animation) of the vocal-fold motion during one oscillation cycle; all parameters as in Fig. 6.

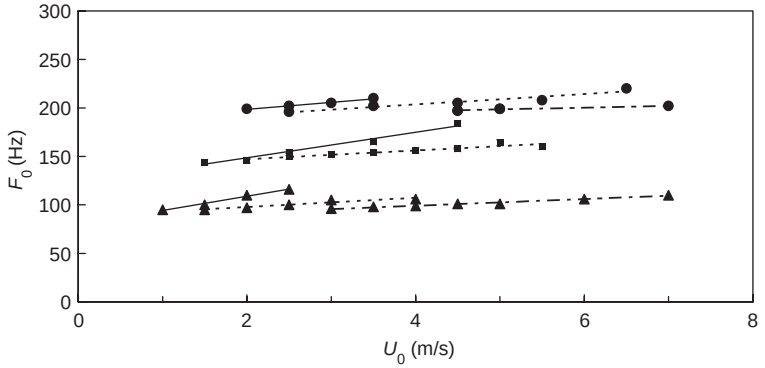

Fig. 9. Fundamental frequency F_0 for self-oscillations versus oncoming flow velocity U_0 for various natural frequencies f_1, f_2 of the vocal-fold model: ▲, $f_1 = 100\,\mathrm{Hz}$, $f_2 = 105\,\mathrm{Hz}$; ■, $f_1 = 150\,\mathrm{Hz}$, $f_2 = 155\,\mathrm{Hz}$; •, $f_1 = 200\,\mathrm{Hz}$, $f_2 = 205\,\mathrm{Hz}$; and for several glottal half-gaps g: —, $g = 0.2\,\mathrm{mm}$; - - -, $g = 0.3\,\mathrm{mm}$; ·····, $g = 0.5\,\mathrm{mm}$.

from Eq. (30). Decreasing subsequently the flow rate from the values $Q > 0.46\,\mathrm{l/s}$, the chaotic oscillations subsisted down to $Q \cong 0.43\,\mathrm{l/s}$, revealing a hysteresis in the values of the phonation instability pressure. Similar, but much smaller hysteresis was observed also for the values of the critical flow rate Q_{crit}. In comparison to the normally expected values of the open quotient measured in human vocal folds, $0 < OQ < 0.5$ (Baken and Orlikoff, 2000), the OQ values from 0 to 0.7 obtained here are reasonable.

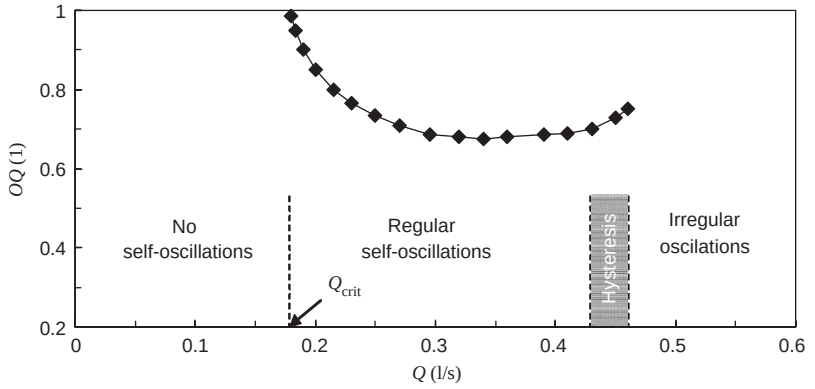

Fig. 10. Open quotient OQ for self-oscillations versus flow volume velocity Q for $f_1 = 100\,\text{Hz}$, $f_2 = 105\,\text{Hz}$ and the glottal half-gap $g = 0.3\,\text{mm}$.

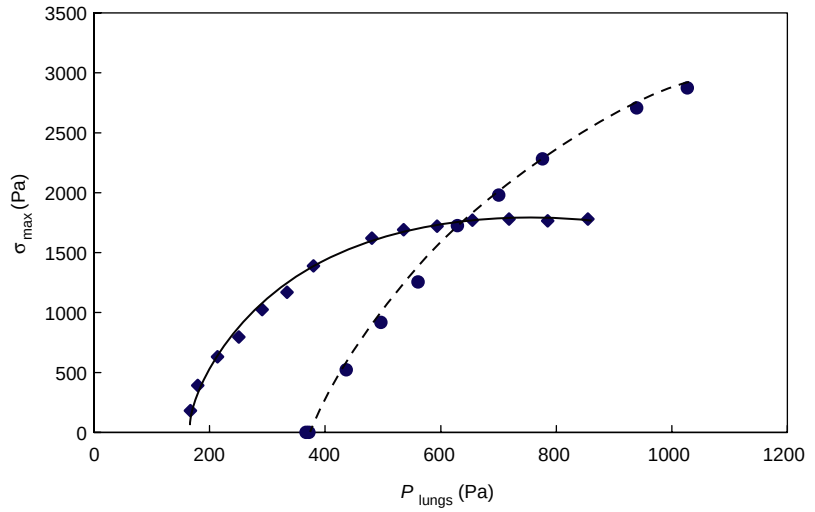

Fig. 11. Maximum impact stress during self-oscillations versus pressure in lungs for $f_1 = 100\,\text{Hz}$, $f_2 = 105\,\text{Hz}$ and the glottal half-gaps: ◆ $g = 0.2\,\text{mm}$; •, $g = 0.5\,\text{mm}$.

Finally, to evaluate the impact forces of the vocal folds resulting from the Hertz model it is useful to relate these to the impact stress, which is easier to measure in the real vocal folds. Impact stress σ (Pa) is defined as the impact force divided by the contact area. The maximum impact stress $\sigma_{\max}$ can be calculated as the maximum value in one oscillation period according to the formula (Brepta and Prokopec, 1972):

$$\sigma_{\max} = \frac{3}{2}\frac{F_{H,\max}}{\pi R^2}, \quad R = \sqrt[3]{\frac{3}{4} r \frac{(1-\nu^2)}{E} F_{H,\max}}, \tag{34}$$

where $F_{H,\max} = \max_{\tau \in \langle t, t+T \rangle} F_H(\tau)$ is the maximum contact force (20) during the oscillatory period T and R is the maximum contact radius.

The calculated results are presented in Fig. 11, where the maximum impact stress $\sigma_{\max}$ is shown for two glottal half-gaps of 0.2 and 0.5 mm as a function of the pressure in the lungs. Each curve begins at a corresponding value of the phonation threshold pressure (P_{th}), at which the impacts are none or very small and thus $\sigma_{\max} \cong 0$, and ends at the phonation instability pressure. The threshold pressure $\sigma_{\max}$ increases with P_{lungs} and reaches its maximum at the phonation instability pressure, where for the smaller g it is possible to see a plateau. The calculated values ($0 < \sigma_{\max} < 3\,\text{kPa}$) for the maximum impact stress in Fig. 11 compare well to the range of the impact stress values

measured on the real vocal folds (Jiang and Titze, 1994; Hess et al., 1998; Verdolini et al., 1999), and indicate that the impact forces implemented in the model are not far from reality.

6. General discussion and conclusion

Perhaps the most dominant feature of the current model advancement is the inclusion of the Hertz model, which expresses the impact force as a function of vocal-fold curvature and material parameters of the vocal-fold tissue. Such a feature is strategically advantageous for studying potential mechanisms of vocal-fold damage through self-exposure to vibration (Titze et al., 2003): thinner vocal folds are generally exposed to different collision forces than thicker vocal folds. In this respect, the Hertz model can be considered more realistic than the abruptly changing of spring stiffness (Ishizaka and Flanagan, 1972), which has been used in other low-order vocal-fold models. The Hertz model is noticeably easier to use than, for example, the finite-element models (Gunter, 2003), but further justification of the Hertz model is needed and the tissue parameters still need more experimental data to rely on. Nevertheless, the good correspondence of the impact stress values reported in human vocal folds with the values calculated here makes the model a promising tool for future investigations of the factors related to vocal-fold collisions.

While the curved surface of the vocal folds is suitable for implementation of the Hertz model of impacts, the mathematical expression of the aerodynamic forces is more complex than in the models with a straight profile between the lower and upper margins of the vocal folds. Consequently, features that are relatively easy to implement in straight-profile vocal-fold models, such as the dependency of the flow-separation point on the divergence of the glottal channel (Pelorson et al., 1994; Lous et al., 1998; Lucero, 1999; Drioli, 2005) require calculating the complex integral functions given in Eq. (14) for every successive time step in this model. The simulations are then highly time-consuming. Fortunately, the flow-separation point is not expected to travel very far from the upper vocal-fold edge in our model, because the particularly curved geometry reduces the divergence of the oscillating glottal channel to only an exit part, which is relatively short. To avoid excessive complexity, the flow-separation point was therefore fixed to the upper vocal-fold edge. Such a simplification appears acceptable here: the calculated stability boundaries approximately correspond to the measured thresholds of phonation in humans and reasonably relate to the conditions and mechanism for starting the vocal-fold vibration. When the instability boundaries for flutter of the aeroelastic system are crossed, the energy transfer from the air-flow to the vocal folds starts to maintain the self-oscillations.

The vibration and stability characteristics obtained for the system studied appear to be important in further research on modelling of the vocal-fold vibration, or in design of artificial aids and vocal-fold replacements for possible use in laryngology. Considering the good correspondence of the model behaviour and its output variables to behaviour and data observed in humans, the model is expected to be useful in studying phenomena and estimating values that are difficult to observe and measure in the living vocal folds.

Acknowledgements

This research has been financially supported by the Grant Agency of the Academy of Sciences of the Czech Republic, Project No. IAA20766401 *Mathematical modelling of human vocal fold oscillations*.

Appendix A

The coefficients $K_i(x)$ $(i = 1, 2, \ldots, 16)$ in Eq. (11) for the pressure $\tilde{p}(x, t)$ on the surface of the vibrating element were calculated using the symbolic manipulation capabilities of the *Mathematica* software and expressed in the following equations:

$$K_1(x) = -\tfrac{1}{2}L_1^2U_0^2[I_3'(L)]^2 + \tfrac{1}{2}L_1^2U_0^2[I_3'(x)]^2 - L_1U_0I_3'(L)I_4'(L) - \tfrac{1}{2}[I_4'(L)]^2 + L_1U_0I_3'(x)I_4'(x) + \tfrac{1}{2}[I_4'(x)]^2, \tag{A.1}$$

$$K_2(x) = U_0\bar{U}(L)I_3'(L) - U_0\sqrt{b^2 - 4ac}\,\bar{U}(x)I_3'(x) - \bar{U}(L)I_5'(L) + \bar{U}(x)I_5'(x), \tag{A.2}$$

$$K_3(x) = -\tfrac{1}{2}U_0^2[I_3'(L)]^2 + \tfrac{1}{2}U_0^2[I_3'(x)]^2 + U_0I_3'(L)I_5'(L) - \tfrac{1}{2}[I_5'(L)]^2 - U_0I_3'(x)I_5'(x) + \tfrac{1}{2}[I_5'(x)]^2, \tag{A.3}$$

$$K_4(x) = -\tfrac{1}{2}[I_1'(L)]^2 + \tfrac{1}{2}[I_1'(x)]^2, \tag{A.4}$$

$$K_5(x) = U_0 I_3(L) - U_0 I_3(x) - I_5(L) + I_5(x) - \bar{U}(L) I'_2(L) + \bar{U}(x) I'_2(x), \tag{A.5}$$

$$K_6(x) = U_0 I'_2(L) I'_3(L) - U_0 I'_2(x) I'_3(x) - I'_2(L) I'_5(L) + I'_2(x) I'_5(x), \tag{A.6}$$

$$K_7(x) = -\tfrac{1}{2}[I'_2(L)]^2 + \tfrac{1}{2}[I'_2(x)]^2, \tag{A.7}$$

$$K_8(x) = -L_1 U_0 I_3(L) + L_1 U_0 I_3(x) - I_4(L) + I_4(x) - \bar{U}(L) I'_1(L) + \bar{U}(x) I'_1(x), \tag{A.8}$$

$$K_9(x) = -L_1 U_0 I'_1(L) I'_3(L) + L_1 U_0 I'_1(x) I'_3(x) - I'_1(L) I'_4(L) + I'_1(x) I'_4(x), \tag{A.9}$$

$$K_{10}(x) = U_0 I'_1(L) I'_3(L) - U_0 I'_1(x) I'_3(x) - I'_1(L) I'_5(L) + I'_1(x) I'_5(x), \tag{A.10}$$

$$K_{11}(x) = -I'_1(L) I'_2(L) + I'_1(x) I'_2(x), \tag{A.11}$$

$$K_{12}(x) = -L_1 U_0 \bar{U}(L) I'_3(L) + L_1 U_0 \bar{U}(x) I'_3(x) - \bar{U}(L) I'_4(L) + \bar{U}(x) I'_4(x), \tag{A.12}$$

$$\begin{aligned} K_{13}(x) = {} & L_1 U_0^2 [I'_3(L)]^2 - L_1 U_0^2 [I'_3(x)]^2 + U_0 I'_3(L) I'_4(L) - U_0 I'_3(x) I'_4(x) - L_1 U_0 I'_3(L) I'_5(L) \\ & - I'_4(L) I'_5(L) + L_1 U_0 I'_3(x) I'_5(x) + I'_4(x) I'_5(x), \end{aligned} \tag{A.13}$$

$$K_{14}(x) = -L_1 U_0 I'_2(L) I'_3(L) + L_1 U_0 I'_2(x) I'_3(x) - I'_2(L) I'_4(L) + I'_2(x) I'_4(x), \tag{A.14}$$

$$K_{15}(x) = -I_1(L) + I_1(x), \quad K_{16}(x) = -I_2(L) + I_2(x), \tag{A.15}$$

where

$$\begin{aligned} & I_1(x) = \frac{1}{2}\int_0^x \xi(\xi - 2L_1)/\bar{H}(\xi)\,\mathrm{d}\xi, \quad I_2(x) = \int_0^x \xi/\bar{H}(\xi)\,\mathrm{d}\xi, \quad I_3(x) = \int_0^x 1/\bar{H}(\xi)\,\mathrm{d}\xi, \\ & I_4(x) = \int_0^x (\xi - L_1)\bar{U}(\xi)/\bar{H}(\xi)\,\mathrm{d}\xi, \quad I_5(x) = \int_0^x \bar{U}(\xi)/\bar{H}(\xi)\,\mathrm{d}\xi; \bar{H}(\xi) = H_0 - a(\xi), \end{aligned} \tag{A.16}$$

$I'_i(x)$ $(i = 1, \ldots, 5)$ are the derivatives of the functions $I_i(x)$ and the mean flow velocity $\bar{U}(x)$ is given by the formula (9).

Appendix B

The elements of aerodynamic mass $\hat{\mathbf{M}}$, damping $\hat{\mathbf{B}}$ and stiffness $\hat{\mathbf{K}}$ matrices in the equations of motion (24) for the linear approximation are given by

$$\hat{\mathbf{M}} = \begin{bmatrix} \dfrac{L}{l}\left(j_1 - \dfrac{1}{2} i_1(1)\right) & 2j_2 - i_2(1) \\ \dfrac{L}{l}\left(j_{10} - \dfrac{1}{2} i_1(1)\right) & 2j_{11} - i_2(1) \end{bmatrix}, \quad \hat{\mathbf{B}} = \begin{bmatrix} \dfrac{L}{l}(2j_3 + j_7 - j_{20}) & 2(j_4 - j_7) + j_{21} \\ \dfrac{L}{l}(2j_{12} + j_{16} - j_{20}) & 2(j_{13} - j_{16}) + j_{21} \end{bmatrix},$$

$$\hat{\mathbf{K}} = \begin{bmatrix} \dfrac{L}{l}(2j_5 + j_8 - j_{22}) & 2(j_6 - j_8) + j_{23} \\ \dfrac{L}{l}(2j_{14} + j_{17} - j_{22}) & 2(j_{15} - j_{17}) + j_{23} \end{bmatrix}, \tag{B.1}$$

where

$$j_1 = \int_0^1 i_1(z)(1 - z)\,\mathrm{d}z, \quad j_2 = \int_0^1 i_2(z)(1 - z)\,\mathrm{d}z, \quad j_3 = \int_0^1 g_1(z)(1 - z)\,\mathrm{d}z, \tag{B.2}$$

$$j_4 = \int_0^1 g_2(z)(1 - z)\,\mathrm{d}z, \quad j_5 = \int_0^1 g_4(z)(1 - z)\,\mathrm{d}z, \quad j_6 = \int_0^1 g_5(z)(1 - z)\,\mathrm{d}z, \tag{B.3}$$

$$j_7 = \int_0^1 i_3(z)(1 - z)\,\mathrm{d}z, \quad j_8 = \int_0^1 g_3(z)(1 - z)\,\mathrm{d}z, \quad j_{10} = \int_0^1 i_1(z) z\,\mathrm{d}z, \tag{B.4}$$

$$j_{11} = \int_0^1 i_2(z) z \, dz, \quad j_{12} = \int_0^1 g_1(z) z \, dz, \quad j_{13} = \int_0^1 g_2(z) z \, dz, \tag{B.5}$$

$$j_{14} = \int_0^1 g_4(z) z \, dz, \quad j_{15} = \int_0^1 g_5(z) z \, dz, \quad j_{16} = \int_0^1 i_3(z) z \, dz, \quad j_{17} = \int_0^1 g_3(z) z \, dz, \tag{B.6}$$

$$i_1(z) = \int_0^z G^{-1}(\xi)\xi(\xi - 1) \, d\xi, \quad i_2(z) = \int_0^z G^{-1}(\xi)\xi \, d\xi, \tag{B.7}$$

$$i_3(z) = \int_0^z G^{-1}(\xi) \, d\xi, \quad i_4(z) = \int_0^z G^{-2}(\xi)\left(\xi - \frac{1}{2}\right) d\xi, \quad i_5(z) = \int_0^z G^{-2}(\xi) \, d\xi, \tag{B.8}$$

$$g_1(z) = i_4(z) + \tfrac{1}{2} G^{-2}(z) z(z - 1), \quad g_2(z) = i_5(z) + G^{-2}(z) z, \tag{B.9}$$

$$g_3(z) = G^{-2}(z), \quad g_4(z) = \left(z - \frac{1}{2}\right) G^{-3}(z) z, \quad g_5(z) = G^{-3}(z), \tag{B.11}$$

$$j_{20} = \tfrac{1}{2} i_3(1) + g_1(1), \quad j_{21} = i_3(1) - g_2(1), \tag{B.12}$$

$$j_{22} = g_4(1) + \tfrac{1}{2} g_3(1), \quad j_{23} = g_3(1) - g_5(1), \tag{B.13}$$

$$G(\xi) = 1 - \frac{a(\xi L)}{H_0}. \tag{B.14}$$

References

Adachi, S., Yu, J., 2005. Two-dimensional model of vocal fold vibration for sound synthesis of voice and soprano singing. Journal of the Acoustical Society of America 117, 3213–3224.

Alipour, F., Berry, D.A., Titze, I.R., 2000. A finite-element model of vocal-fold vibration. Journal of the Acoustical Society of America 108, 3003–3012.

Baken, R.J., Orlikoff, R., 2000. Clinical Measurement of Speech and Voice, second ed. Singular.

Berry, D.A., 2001. Mechanism of modal and non-modal phonation. Journal of Phonetics 29, 431–450.

Berry, D.A., Titze, R., 1996. Normal modes in continuum model of vocal fold tissues. Journal of the Acoustical Society of America 100, 3345–3354.

Berry, D.A., Herzel, H., Titze, R., Krischer, K., 1994. Interpretation of biomechanical simulations of normal and chaotic vocal fold oscillations with empirical eigenfunctions. Journal of the Acoustical Society of America 95, 3595–3604.

Brepta, R., Prokopec, M., 1972. Wave Propagation and Impacts in Solids. Academia, Praha (in Czech).

Cancelli, C., Pedley, T.J., 1985. A separated-flow model for collapsible-tube oscillations. Journal of Fluid Mechanics 157, 375–404.

Chan, R.W., Titze, I.R., Titze, M.R., 1997. Further studies of phonation threshold pressure in a physical model of the vocal fold mucosa. Journal of the Acoustical Society of America 101, 3722–3727.

Deverge, M., Pelorson, X., Vilain, C., Lagree, P.Y., Chentouf, F., Willems, J., Hirschberg, A., 2003. Influence of collision on the flow through in-vitro rigid models of the vocal folds. Journal of the Acoustical Society of America 114, 3354–3362.

De Vries, M.P., Schutte, H.K., Verkerke, G.J., 1999. Determination of parameters for lumped parameter models of the vocal folds using a finite-element method approach. Journal of the Acoustical Society of America 106, 3620–3628.

Drioli, C., 2005. A flow waveform-matched low-dimensional glottal model based on physical knowledge. Journal of the Acoustical Society of America 117, 3184–3195.

Gunter, H.E., 2003. A mechanical model of vocal-fold collision with high spatial and temporal resolution. Journal of the Acoustical Society of America 113, 994–1000.

Herzel, H., Knudsen, C., 1995. Bifurcations in a vocal fold model. Nonlinear Dynamics 7, 53–64.

Hess, M.M., Verdolini, K., Bierhals, W., Mansmann, U., Gross, M., 1998. Endolaryngeal contact pressures. Journal of Voice 12, 50–67.

Horáček, J., Švec, J.G., 2002a. Aeroelastic model of vocal-fold-shaped vibrating element for studying the phonation threshold. Journal of Fluids and Structures 16, 927–951.

Horáček, J., Švec, J.G., 2002b. Instability boundaries of a vocal fold modelled as a flexibly supported rigid body vibrating in a channel conveying fluid. In: Proceedings of the Fifth International Symposium on FSI, AE and FIV + N, 2002 ASME International Mechanical Engineering Congress, November 2002, New Orleans, Louisiana, USA, IMECE 2002-32285, pp. 17–22.

Ikeda, T., Matsuzaki, Y., Aomatsu, T., 2001. A numerical analysis of phonation using a two-dimensional flexible channel model of the vocal folds. ASME Journal of Biomechanical Engineering 123, 571–579.

Ishizaka, K., Flanagan, J.L., 1972. Synthesis of voiced sounds from a two-mass model of the vocal cords. The Bell System Technical Journal 51, 1233–1268.

Jiang, J., Titze, I., 1993. A methodological study of hemilaryngeal phonation. Laryngoscope 103, 872–882.

Jiang, J., Titze, I., 1994. Measurement of vocal fold intraglottal pressure and impact stress. Journal of Voice 8, 132–144.

Jiang, J.J., Zhang, Yu., Ford, Ch.N., 2003. Nonlinear dynamics of phonations in excised larynx experiments. Journal of the Acoustical Society of America 114, 2198–2205.

Kaneko, T., Uchida, K., Suzuki, H., Komatsu, K., Kanesaka, T., Kobayashi, N., Naito, J., 1981. Mechanical properties of the vocal fold: measurement in vivo. In: Stevens, K.N., Hirano, M. (Eds.), Vocal Fold Physiology. University of Tokyo Press, Tokyo, pp. 365–376.

Kaneko, T., Komatsu, K., Suzuki, H., Kanesaka, T., Masuda, T., Numata, T., Naito, J., 1983. Mechanical properties of the human vocal fold resonance characteristics in living humans and in excised larynges. In: Titze, I.R., Scherer, R.C. (Eds.), Vocal Fold Physiology: Biomechanics, Acoustics and Phonatory Control. The Denver Center for the Performing Arts, Denver, CO, USA, pp. 304–317.

Kaneko, T., Masuda, T., Shimada, A., Suzuki, H., Hayasaki, K., Komatsu, K., 1987. Resonance characteristics of the human vocal fold in vivo and in vitro by an impulse excitation. In: Baer, T., Sasaki, C., Harris, K.S. (Eds.), Laryngeal Function in Phonation and Respiration. A College-Hill Press, Little, Brown and Company, Boston, pp. 349–365.

Kob, M., 2002. Physical Modelling of the Singing Voice. Logos-Verlag, Berlin.

LaMar, M.D., Qi, Y., Xin, J., 2003. Modeling vocal fold motion with a hydrodynamic semicontinuum model. Journal of the Acoustical Society of America 114, 455–464.

Liljencrants, J., 1991. A translating and rotating mass model of the vocal folds. In: Speech Transmission Laboratory—Quarterly Progress and Status Report 1/1991, Stockholm, Sweden, pp. 1–18

Lous, N.J.C., Hofmans, G.C.J., Veldhuis, R.N.J., Hirschberg, A., 1998. A symmetrical two-mass vocal-fold model coupled to vocal tract and trachea, with application to prosthesis design. Acustica—Acta Acustica 84, 1135–1150.

Lucero, J.C., 1999. A theoretical study of the hysteresis phenomenon at vocal fold oscillation onset–offset. Journal of the Acoustical Society of America 105, 423–431.

Norton, M.P., 1989. Fundamentals of Noise and Vibration Analysis for Engineers. Cambridge University Press, Cambridge.

Pelorson, X., Hirschberg, A., Van Hasse, R.R., Wijnands, A.P.J., Auregan, Y., 1994. Theoretical and experimental study of quasisteady-flow separation within the glottis during phonation. Application to a modified two-mass model. Journal of the Acoustical Society of America 96, 3416–3431.

Půst, L., Peterka, F., 2003. Impact oscillator with Hertz's model of contact. Meccanica 38, 99–114.

Schutte, H.K., 1980. The efficiency of voice production. Doctoral dissertation, Groningen.

Sciamarella, D., d'Alessandro, C., 2004. On the acoustic sensitivity of a symmetrical two-mass model of the vocal folds to the variation of control parameters. Acta Acustica united with Acustica 90, 746–761.

Story, B.H., Titze, I.R., 1995. Voice simulation with a body cover model of the vocal folds. Journal of the Acoustical Society of America 97, 1249–1260.

Stronge, W.J., 2000. Impact Mechanics. Cambridge University Press, Cambridge, UK.

Švec, J.G., Horáček, J., Šram, F., Veselý, J., 2000. Resonance properties of the vocal folds: in vivo laryngoscopic investigation of the externally excited laryngeal vibrations. Journal of the Acoustical Society of America 108, 1397–1407.

Thomson, S.L., Mongeau, L., Frankel, S.H., 2003. Physical and numerical flow-excited vocal fold models. In: Third International Workshop MAVEBA 2003, Firenze University Press, pp. 147–150.

Titze, I.R., 1989. Physiologic and acoustic differences between male and female voices. Journal of the Acoustical Society of America 85, 1699–1707.

Titze, I.R., 1992. Phonation threshold pressure: a missing link in glottal aerodynamics. Journal of the Acoustical Society of America 91, 2928–2934.

Titze, I.R., Švec, J.G., Popolo, P.S., 2003. Vocal dose measures: quantifying accumulated vibration exposure in vocal fold tissues. Journal of Speech, Language and Hearing Research 46, 919–932.

Verdolini, K., Hess, M.M., Titze, I.R., Bierhals, W., Gross, M., 1999. Investigation of vocal fold impact stress in human subjects. Journal of Voice 13, 184–202.

Wolfram, S., 2003. The Mathematica Book, fifth ed. Wolfram Media.